# Multiple graphene-layer-based heterostructures with van der Waals barrier layers for terahertz superluminescent and laser diodes with lateral/vertical current injection


doi: 10.1088/1361-6641/ab9398

# Multiple graphene-layer-based heterostructures with van der Waals barrier layers for terahertz superluminescent and laser diodes with lateral/vertical current injection

**V Ryzhii[1,2,3,4], M Ryzhii[5], T Otsuji[1], V E Karasik[3], V Leiman[4], V Mitin[6], and M S Shur[7]**

[1]Research Institute of Electrical Communication, Tohoku University, Sendai 980-8577, Japan
[2]Institute of Ultra High Frequency Semiconductor Electronics, RAS, Moscow 117105, Russia
[3]Center for Photonics and Infrared Engineering, Bauman Moscow State Technical University, Moscow 111005, Russia
[4]Center for Photonics and Two-Dimensional Materials, Moscow Institute of Physics and Technology, Dolgoprudny 141700, Russia
[5]Department of Computer Science and Engineering, University of Aizu, Aizu-Wakamatsu 965-8580, Japan
[6]Department of Electrical Engineering, University at Buffalo SUNY, Buffalo, NY 14260-1920, USA
[7]Departments of Electrical, Computer, and Systems Engineering and Physics, Applied Physics, and Astronomy, Rensselaer Polytechnic Institute, Troy, NY 12180, USA

E-mail: v-ryzhii@riec.tohoku.ac.jp

**Abstract.** We analyze terahertz superluminescent and laser diodes using the injection pumping in the multiple graphene-layer (GL)/van der Waals barrier layers (BLs) heterostructures. The operation of such terahertz radiation sources is associated with the interband transitions in the gapless GLs under the population inversion leading to the GL negative dynamic conductivity. These devices use the lateral injection of holes and vertical injection of electrons. Such an injection might have advantages over the lateral injection of the bipolar carriers. Due to relatively large conduction band offsets at the GL-BL interface, the population inversion at the vertical injection can be markedly hampered by the injection current heating of the two-dimensional electron-hole plasma (2DEHP) in the GLs. We show that doping GLs and/or BLs can substantially diminish the carrier heating promoting the interband population. Numerical analysis assumed the BL material parameters of $MoS_2$ and $WSe_2$ and showed the feasibility of such terahertz radiation sources.

*Keywords*: graphene, van der Waals, injection, super-luminescence, terahertz
Submitted to: *Semicond. Sci. Technol.*

## 1. Introduction

Application of the graphene layers (GLs) and GL-based heterostructures in the terahertz (THz) and far-infrared (FIR) photodetectors, luminescent and laser sources has attracted a lot of attention (see, for example, the reviews [1–5]). The lateral double carrier injection (in the GL plane) [6, 7] could provide the interband population inversion which, in turn, could lead to a negative dynamic conductivity. The GL-based heterostructure with lateral carrier injection and the grating providing the distributed feedback demonstrated a single-mode lasing at 5.2 THz and a broadband (1-8 THz) amplied spontaneous emission, both at 100 K [8–10]. One of the advantages of the lateral injection in the GL-based heterostructures (in comparison with the optical pumping using mid-infrared, near-infrared, and visible light sources [11–18]) is the generation in the GLs the two-dimensional electron-hole plasma (2DEHP) with only moderate Joule heating [19]. However, the potential sag between the side contacts [19] and, hence, relatively low carrier densities in the middle of the structures (the effect analogous to the current-crowding effect in bipolar transistors [20, 21]) limits the efficiency of the lateral pumping. Recently [22], we proposed to use the combined injection pumping: the lateral injection of electrons (or holes) and the vertical injection of the carriers opposite polarity (similar to the pumping scheme used in light-emitting diodes and heterostructure lasers operating in shorter wavelength ranges). This allows to avoid the 2DEHP lateral nonuniformity. The implementation of the vertical injection with no heating (or even with cooling) requires to use the BLs sandwiching the GL (or GLs) to provide a relatively low barriers for the electrons and holes, $\Delta_C$ and $\Delta_V$, residing in the GL. The pertinent condition is $\Delta_C < \hbar\omega_0$ (for the electron vertical injection) or $\Delta_V < \hbar\omega_0$ (for the hole vertical injection). Here $\hbar\omega_0 \simeq 200$ meV is the optical phonon energy in GLs.

The black-Phosphorus (b-P), black-Arsenic (b-As), and black-AsP compounds [23–37] are the examples of such BL materials. The energy spacing between the GL Dirac point and the edges of the conduction and valence bands, $\Delta_C$ and $\Delta_V$, are $\Delta_C \simeq 200$ meV and $\Delta_V \simeq 100$ meV for the b-P and $\Delta_C \simeq 100$ meV and $\Delta_V = 50$ meV for b-As [38, 39]. Hence, these BLs satisfy the vertical hole injection requirements. Other, including the van der Waals (vdW) materials, have larger band offsets: $\Delta_C, \Delta_V > \hbar\omega_0$. For example, the band alignment of GLs and $MoS_2$ and $WSe_2$ BLs corresponds to $\Delta_C \simeq 0.35$ eV and $\Delta_C \simeq 0.54$ eV, respectively [40–43]. The heating of the 2DEHP by the vertically injected electrons in the heterostructures with the BLs made of such materials might prevent the population inversion formation. However. in this paper, we show that the THz superluminescent and laser diodes based on the GL-$MoS_2$ and GL-$WSe_2$ heterostructures could be implemented using the combined vertical/lateral injection and a strong GL doping to minimize the 2DEHP heating.

## 2. Device structure

The device structure under consideration comprises one or several p-doped GLs separated by the inter-GL BLs (see figure 1). The GLs are supplied with the side contacts $p^+$-injecting contacts. The $n^+$-n region of the same BL material on the top of the heterostructure serves as the vertical electron injector operating in the regime of the space-charge-limited injection (see the band diagram in figure 1(b)). The injected electrons diffuse across the barriers

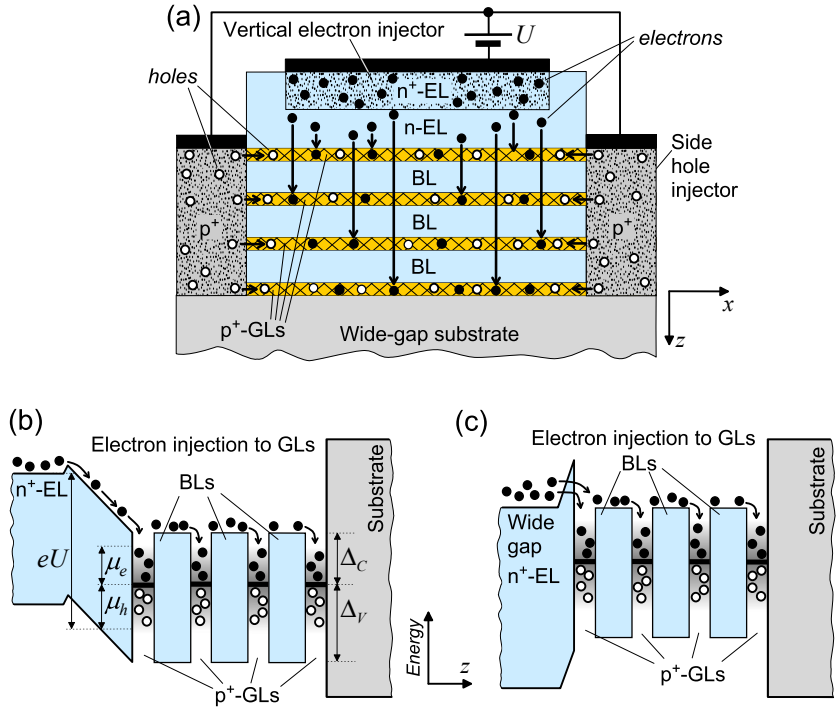


**Figure 1.** Schematic views of (a) the multiple-GL-based heterostructure with vertical injection of electrons and lateral injection of holes, (b) the energy band diagram of the heterostructures with the electron space-charge or electron scattering limited injection, and (c) with the electron tunneling injection.

and are captured in the GLs due to electron-hole interactions, the interactions with acoustic and optical phonons [44, 45]. Small variations of the potential across the BLs, particularly across the BL adjacent to the n-EL, caused some electron-hole imbalance are neglected. Figure 1(c) shows the band structure of the device with the tunneling hole injection from the $N^+$ region made of relatively wide-gap material. As demonstrated in figures 1(b) and 1(c), the injected electrons are coming to the GLs with some extra energy. This energy is distributed among the all components of the 2DEHP. Thus, the injection provides not only an increase in the electron and hole densities in the 2DEHP but also affects the electron and hole distributions. The p-doping of the GLs can result in substantially higher hole densities in comparison with the electron densities.

## 3. Main equations of the model

Our mathematical model (which generalizes that used previously [22], see also [7, 46]) is based on the equations governing the balance of the interband and intraband energy relaxation and the recombination-generation processes in the GLs (see Appendix A). The model assumes that these processes at the temperature under consideration (room temperature or somewhat lower) are associated with the GL optical phonons in the GLs [47]. The model accounts for the energy of the 2DEHP decrease or increase in each act of the optical phonon emission or absorption.

The density of the vertically injected electrons is spatially nonuniform (decreasing from the the emitter toward the substrate). We assume that the number of the GLs $N$ is not too large, so that the electron non-

uniformity across the heterostructure can be disregarded (see Appendix B). In such a situation, the capture rate into all the GLs is approximately equal to $j/eN$, where $j$ is the density of vertically injected current and $e = |e|$ is the electron charge. We also disregard heating of the optical phonon system and set their distribution as $\mathcal{N}_0 = [\exp(\hbar\omega_0/T_0) - 1]^{-1}$ with $T_0$ being the lattice (thermostat) temperature. This is justified by a relatively short time of the optical phonon decay t into acoustic pjonons in the GLs [48] and by a high GL heat conductivity [49, 50].

Due to fairly high GL carrier densities at the interband population inversion, the frequent inter-carrier collisions result in the establishment of the common effective temperature $T$ of the 2DEHP electrons and holes due to the relatively long times of establishement the interband equilibrium. However, the electrons and holes components are characterized by the quasi-Fermi energies, $\mu_e$ and $\mu_h$ with generally $\mu_e \neq -\mu_h$ due to the relatively long times of establishing the interband equilibrium. A similar situation is typical for the standard superluminescent and laser diodes using the interband transitions. Hence, from the rate equations in the Appendix A one can arrive at:

$$\frac{1}{\tau_0^{inter}}\left\{\exp\left(\frac{\mu_e+\mu_h}{T}\right)\exp\left[\hbar\omega_0\left(\frac{1}{T_0}-\frac{1}{T}\right)\right]-1\right\} = \frac{j}{e\Sigma_0 N}, \tag{1}$$

$$\frac{1}{\tau_0^{inter}}\left\{\exp\left(\frac{\mu_e+\mu_h}{T}\right)\exp\left[\hbar\omega_0\left(\frac{1}{T_0}-\frac{1}{T}\right)\right]-1\right\} + \frac{1}{\tau_0^{intra}}\left\{\exp\left[\hbar\omega_0\left(\frac{1}{T_0}-\frac{1}{T}\right)\right]-1\right\} = \frac{j}{e\Sigma_0 N}\left(\frac{\Delta_i}{\hbar\omega_0}\right). \tag{2}$$

Here $T$ is the carrier effective temperature (in the energy units) in the GLs, $\Sigma_0$ is the characteristic carrier density determined by the energy dependence of the density of state in the GL near the Dirac point, $\tau_0^{inter}$ and $\tau_0^{intra}$ are the characteristic recombination and intraband relaxation times associated with the carrier interaction with the optical phonons, $\Delta_i$ is the average energy bringing by the hole injected from the EL to the GL. The quantity $j_G/e = \Sigma_0/\tau_0^{inter}$ is the order of the equilibrium electron-hole pair thermogeneration rate per unit area [48], so that $\tau_0^{inter} \sim \tau_0 \exp(\hbar\omega_0/T_0)$, where $\tau_0$ is the time of the optical phonon spontaneous emission. The ratio $\eta_0 = \tau_0^{intra}/\tau_0^{inter}$ is determined by the energy dependence of the GL density of state (which is a linear function). The quantity $\eta_0$ as a function of the carrier Fermi energies and their effective temperatures can be interpolated as [7, 46]

$$\eta_0 \simeq \frac{\hbar^2\omega_0^2}{[3(\mu_e^2+\mu_h^2)+\pi^2T^2]}. \tag{3}$$

A decrease in $\tau_0^{intra}$ and, hence, in the parameter $\eta_0$ with increasing $\mu_e^2$ and $\mu_h^2$ is due to the proportionality of these quantities to the densities of the pertinent carriers: at high densities $\Sigma_e \propto \mu_e^2$ and $\Sigma_h \propto \mu_h^2$. The dependence of $\eta_0$ on the electron and hole quasi-Fermi energies can be crucial for high densities, particularly, for the heavy doped GLs.

The injected energy $\Delta_i$ is determined by the BL height $\Delta_C$ (i.e., by the pertinent band-offset), the effective temperature of the injected electrons $T_E \simeq T_0$, and the fraction of the energy transferred to the 2DEHP due to the injected electrons capture into the GLs. This fraction can be estimated considering that the captured electron can lose its energy due to the collisions with the thermalized carriers and by emitting one or several optical phonons. In the first case, the total injected electron energy

$\Delta_C + 3T_E/2$ transfers to the 2DEHP. In the second mechanism, the energy receiving by the 2DEHP is $\Delta_C + 3T_E/2 - K\hbar\omega_0$. Here $K$ is the number of optical phonons emitted by the injected electron before its thermalization (the number of the optical phonon cascade): $K < \Delta_C/\hbar\omega_0 < K+1$. Taking into account that the ratio of the probabilities of the inter-carrier scattering and the optical phonon intraband emission is $\eta_{cc} = \tau_0^{intra}/\tau_{cc}$, one can set (compare with [46])

$$\Delta_i \simeq \Delta_C + \frac{3T_E}{2} - \frac{K\hbar\omega_0}{(1+K\eta_{cc})}. \tag{4}$$

In line with the previous calculations [45], the parameter $\eta_{cc}$ can be estimated as $\eta_{cc} \sim 1$, so that $\Delta_i$ can be markedly smaller than $\Delta_C$.

Equations (1) - (3) yield

$$\frac{T_0}{T} = 1 - \frac{T_0}{\hbar\omega_0}\ln\Big[1 + \frac{\hbar^2\omega_0^2\Big(\frac{\Delta_i}{\hbar\omega_0} - 1\Big)\frac{j}{Nj_G}}{3(\mu_e^2+\mu_h^2)+\pi^2T^2}\Big] \tag{5}$$

$$\frac{\mu_e+\mu_h}{T} = \hbar\omega_0\Big(\frac{1}{T} - \frac{1}{T_0}\Big) + \ln\Big(1 + \frac{j}{Nj_G}\Big). \tag{6}$$

Due to the quasi-neutrality of the 2DEHP (the electron, hole, and acceptor densities $\Sigma_e$, $\Sigma_h$, and $\Sigma_a$ in each GL are related as $\Sigma_h - \Sigma_e = \Sigma_a$), the electron and hole quasi-Fermi energies, $\mu_e$ and $\mu_h$ obey the following relation:

$$\Big(\frac{T}{T_0}\Big)^2\Big[\int_0^\infty \frac{d\varepsilon\varepsilon}{1+\exp(\varepsilon-\mu_h/T)} - \int_0^\infty \frac{d\varepsilon\varepsilon}{1+\exp(\varepsilon-\mu_e/T)}\Big] = \frac{\Sigma_a}{\Sigma_{00}}. \tag{7}$$

Here $\Sigma_{00} = 2T_0^2/\pi\hbar^2v_W^2$, $\hbar$ is the reduced Plank constant, $v_W \simeq 10^8$ cm/s is the characteristic velocity of electrons and holes in GLs. For the interband superluminescence or lasing, at least the electron component should be degenerate $\mu_h \gg T$. In the case of the degeneracy of both the electrons and holes in the 2DEHP, at a sufficiently strong injection, $\mu_e \simeq \hbar\, v_W\sqrt{\pi\Sigma_e}$ and $\mu_h \simeq \hbar\, v_W\sqrt{\pi(\Sigma_h+\Sigma_a)}$. This leads to the following equation supplementing equation (5):

$$\mu_h^2 - \mu_e^2 = \mu_a^2 \tag{8}$$

with $\mu_a = \hbar\, v_W\sqrt{\pi\Sigma_a}$. In such a case,

$$\mu_e^2 + \mu_h^2 = \frac{(\mu_e+\mu_h)^2}{2} + \frac{2\mu_a^4}{(\mu_e+\mu_h)^2}. \tag{9}$$

## 4. Population inversion

The interband population inversion in the GLs corresponds to the positive parameter $\zeta = (\mu_e+\mu_h)/T$.

If the GLs are undoped and at a weak injection ($\mu_e, \mu_h \ll T_0$) equation (5) yields

$$\frac{T}{T_0} \simeq 1 + \frac{\hbar\omega_0}{\pi^2T_0^2}\Big(\frac{\Delta_i}{\hbar\omega_0} - 1\Big)\frac{j}{Nj_G}. \tag{10}$$

As follows from equation (10), in the heterostructures with $\Delta_i < \hbar\omega_0$, the 2DEHP effective temperature decreases with increasing injection current becoming smaller that the lattice temperature $T_0$ (the 2DEHP cooling by the injected current). In this case, equation (6) yields $(\mu_e+\mu_h) \geq 0$ with a rise of $\zeta$ when the injected current $j$ increases.

If $\Delta_i < \hbar\omega_0$, $T$ increases with increasing $j$. However, in such a case, $(\mu_e+\mu_h)$ can be both positive or negative depending on $(\Delta_i/\hbar\omega_0 - 1)$ and, what is important, on $\mu_a$, i.e., on the GL doping level.

For the BL materials under consideration, setting $\Delta_C = 350$ meV ($MoS_2$) and $\Delta_C = 540$ meV ($WSe_2$), $\hbar\omega_0 = 200$ meV, $T_0 = 26$ meV, and $\eta_{cc} = 1$, we obtain $\Delta_i \simeq 289$ meV and $\Delta_i = 446$ meV, respectively. In particular, if $\mu_a = 0$ for the case of the undoped $MoS_2$ BLs ($\mu_a = 0$), for the population inversion parameter one obtains $\zeta \simeq -1.67j/Nj_G < 0$. But, as demonstrated

in the following, the GL doping can change the sign of the population inversion parameter $\zeta$ from negative to positive. The parameter $\zeta$ has to be relatively large in order to reach the pronounced population inversion. This requires a sufficiently strong injection level. In this case, both electron and hole components are degenerate, so that, using equation (9) and introducing the normalized temperature $\Theta = T/T_0$, equations (5) and (6) can be reduced to

$$\ln\left\{1+\frac{\left(\frac{\hbar\omega_0}{T_0}\right)^2\left(\frac{\Delta_i}{\hbar\omega_0}-1\right)}{\Theta^2\left[\pi^2+3\left(\frac{\zeta^2}{2}+\frac{2\mu_a^4}{T_0^4\zeta^2\Theta^2}\right)\right]}\frac{j}{Nj_G}\right\}$$
$$+\frac{\hbar\omega_0}{T_0}\left(\frac{1}{\Theta}-1\right)=0, \qquad (11)$$

$$\zeta=\frac{\hbar\omega_0}{T_0}\left(\frac{1}{\Theta}-1\right)+\ln\left(1+\frac{j}{Nj_G}\right). \qquad (12)$$

Equations (11) and (12) contain the following parameters : $\hbar\omega_0/T_0$, $\mu_a/T_0$, and $\Delta_i/\hbar\omega_0$.

Figure 2 shows the 2DEHP normalized effective temperature $\Theta = T/T_0$ versus the normalized injected current $j/Nj_G$ calculated numerically using equations (11) and (12) for the GL–$MoS_2$ with different GL doping levels (different values of $\mu_a$) and $T_0 = 26$ meV. This figure confirms the qualitative reasoning that an increase in the doping level leads to a substantially slower rise of the 2DEHP effective temperature as a function of the injection current. This is beneficial for the reinforcement of the population inversion.

Figure 3 shows the population inversion parameter $\zeta$ as a function of the normalized injected current $j/Nj_G$ calculated numerically using equations (11) and (12) for both GL–$MoS_2$ and GL-$WSe_2$ heterostructures for the same doping levels as in figure 2. In particular, the calculations show that for the undoped GLs ($\mu_a = 0$), $\zeta < 0$ for all densities of the injected current. As seen from figure 3, for undoped GLs (see the curves "1" for $\mu_a = 50$ meV) at small injection currents $\zeta < 0$ in line with equation (10) (and the related comments after this equation), but at larger currents $\zeta$ can change its sign. This can be attributed to relatively large 2DEHP densities at a strong injection (even without doping). However, in this case, $\zeta$ is fairly small, meaning no marked interband population inversion in the heterostructures under consideration occurs. The data shown in figure 3 for the sufficiently strong GL doping, correspond to positive and large $\zeta$ that corresponds to the pronounced interband population inversion in the GLs, at least at $\mu_a \geq 50$ meV.

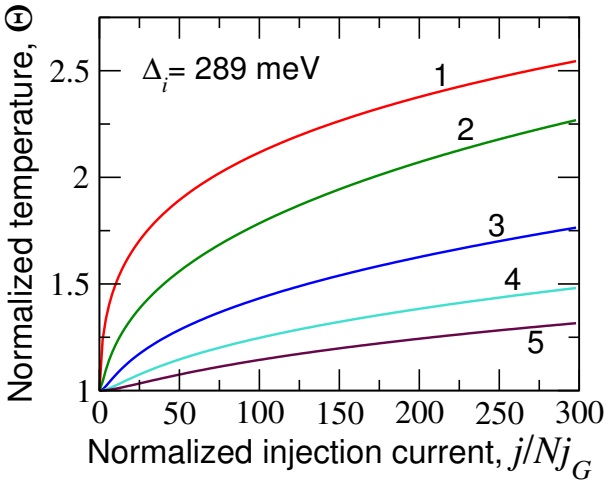


**Figure 2.** Normalized effective temperature $\Theta = T/T_0$ versus normalized injection current $j/Nj_G$ in GL-$MoS_2$ heterostructures with different GL doping levels: 1 - $\mu_a = 0$, 2 - $\mu_a = 50$ meV, 3 - $\mu_a = 100$ meV, 4 - $\mu_a = 150$ meV, and 5 - $\mu_a = 200$ meV.

## 5. Dynamic conductivity

The interaction of the photon and plasmon modes propagating along the y-direction (see figure 1(a)) with the 2DEHP in the GLs is determined by the $xx-$ and $yy-$ components of the tensor of the GL dynamic

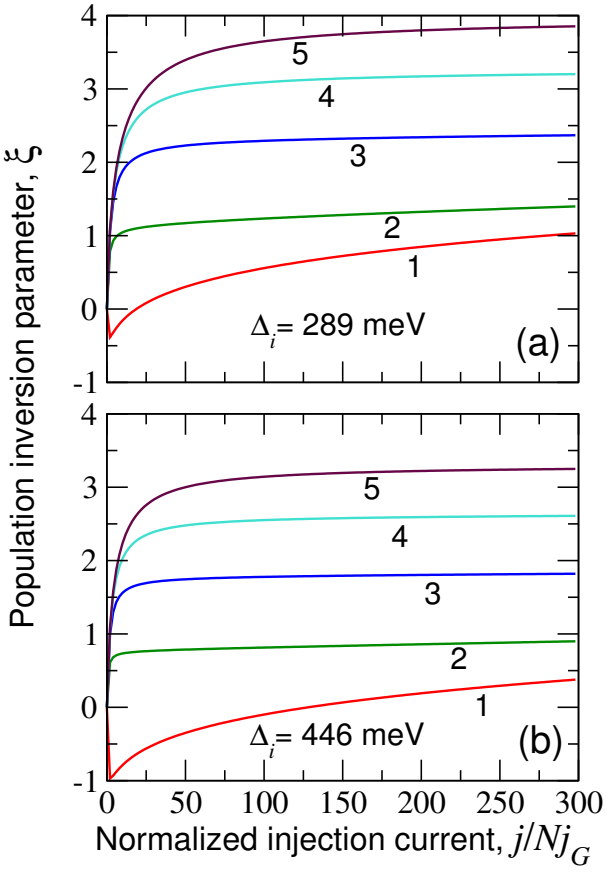


**Figure 3.** Population inversion parameter $\zeta = (\mu_e + \mu_h)/T$ versus normalized injection current $j/Nj_G$ in (a) GL-$MoS_2$ and (b) GL-$WSe_2$ heterostructures with different GL doping levels: 1 - $\mu_a = 0$, 2 - $\mu_a = 50$ meV, 3 - $\mu_a = 100$ meV, 4 - $\mu_a = 150$ meV, and 5 - $\mu_a = 200$ meV (the same as in figure 2).

conductivity. The localization of these modes in the z-direction is usually larger than the heterostructure thickness $Nd$ [13]. In such a case, the conductivities of all GLs are approximately the same (if neglecting the vertical nonuniformity of the injected electron density), and the gain-mode overlap is given by the net dynamic conductivity $\sigma_\omega = \Sigma_{n=1}^{N}\sigma_{\omega,n} \simeq N\sigma_{\omega,GL}$. Here $\sigma_{\omega,GL}$ is the dynamic conductivity of a single GL. The latter is determined by the contributions of the direct interband optical transitions and the intraband radiative transitions assisted with the carrier scattering (leading to the Drude absorption): $\sigma_{\omega,GL}^{inter} = \mathrm{Re}\sigma_{\omega,GL}^{inter} + \mathrm{Im}\sigma_{\omega,GL}^{inter}$ and $\sigma_{\omega,GL}^{intra} = \mathrm{Re}\sigma_{\omega,GL}^{intra} + \mathrm{Im}\sigma_{\omega<GL}^{intra}$. Hence, the interband contribution of the real part of the net dynamic conductivity, $\mathrm{Re}\sigma_\omega^{inter}$, of the heterostructure with $N$ GLs can be found as in [11, 12, 51]:

$$\mathrm{Re}\sigma_\omega^{inter} = \frac{N\left(\frac{e^2}{4\hbar}\right)\sinh\left[\frac{\hbar\omega-(\mu_e+\mu_h)}{2T}\right]}{\cosh\left[\frac{\hbar\omega-(\mu_e+\mu_h)}{2T}\right]+\cosh\left(\frac{\mu_e-\mu_h}{2T}\right)} = \frac{N\left(\frac{e^2}{4\hbar}\right)\sinh\left[\frac{\hbar\omega-(\mu_e+\mu_h)}{2T}\right]}{\cosh\left[\frac{\hbar\omega-(\mu_e+\mu_h)}{2T}\right]+\cosh\left[\frac{\mu_d^2}{2(\mu_e+\mu_h)T}\right]}. \quad (13)$$

In the case of undoped GLs ($\mu_d = 0$ and $\mu_e = \mu_h = \mu$), equation (13) yields the standard formula [11]:

$$\mathrm{Re}\sigma_\omega^{inter} = N\left(\frac{e^2}{4\hbar}\right)\tanh\left(\frac{\hbar\omega-2\mu}{4T}\right). \quad (14)$$

Equation (13) can be rewritten using the dimensionless parameters $\Theta$ and $\zeta$ introduced above:

$$\mathrm{Re}\sigma_\omega^{inter} = \frac{N\left(\frac{e^2}{4\hbar}\right)\sinh\left(\frac{\hbar\omega}{2T_0}\frac{1}{\Theta}-\frac{\zeta}{2}\right)}{\cosh\left(\frac{\hbar\omega}{2T_0}\frac{1}{\Theta}-\frac{\zeta}{2}\right)+\cosh\left(\frac{\mu_d^2}{2T_0^2\zeta\Theta^2}\right)} \quad (15)$$

As seen from equation (15), the heterostructures with a large number of the GLs $N$ exhibit proportionally reinforcement of the effect of negative dynamic conductivity. However, an increase in the absolute value of the dynamic conductivity with increasing $N$ is limited by the nonuniform pumping of the GLs and by the Joule heating.

The intraband contributions to the real part of the GL net dynamic conductivity $\sigma_\omega^{intra}$ markedly depends on the carrier momentum relaxation mechanisms in the GL, particularly,

on the carrier-carrier interactions and the carrier interaction with disorder. At fairly high carrier densities inherent for the heterostructures under consideration the short-range scattering (in particular, on the strongly screened donors) dominates [53–57]. In this case, the real part of the inraband conductivity is given by [58]

$$\mathrm{Re}\sigma_\omega^{intra} \simeq N\xi\Big(\frac{e^2}{4\hbar}\Big)\frac{8\tau_p T_0}{\pi\hbar(1+\omega^2\tau_p^2 3/\pi^2)}, \qquad (16)$$

where $\tau_p$ is the characteristic scattering time of carriers on point scatterers and

$$\xi = \Big[\frac{1}{\exp(-\mu_e/T)+1} + \frac{1}{\exp(-\mu_h/T)+1}\Big].$$

At a relatively strong hole injection, the factor $\xi$ varies from $\xi \simeq 3/2$ if $\mu_e \gg T$ and $\mu_h \sim T$, to $\xi \simeq 2$ if $\mu_e, \mu_h \gg T$. A weak dependence of Re $\sigma_\omega^{intra}$ on the quasi-Fermi energies is due to the short-range carrier scattering in the GL heterostructures under consideration.

If the dominant scattering mechanism of the electrons and holes in the GL is associated with their mutual scatterings, the quantity $\tau_p$ calculated for $T_0 = 26$ meV and $\kappa = 6$ (for a GL sandwiched between the GL and hBN) is about of $\tau_p = 3.6$ ps [58]. To account for other scattering mechanisms (such as impurity and acoustic phonons scattering), we set $\tau_p = 1$ ps.

Using equations (15) and (16), we arrive at

$$\frac{\mathrm{Re}\sigma_\omega^{inter}}{\mathrm{Re}\sigma_\omega^{intra}} = \frac{\sinh\Big(\dfrac{\hbar\omega}{2T_0}\dfrac{1}{\Theta} - \dfrac{\zeta}{2}\Big)}{\cosh\Big(\dfrac{\hbar\omega}{2T_0}\dfrac{1}{\Theta} - \dfrac{\zeta}{2}\Big) + \cosh\Big(\dfrac{\mu_d^2}{2T_0^2\zeta\Theta^2}\Big)} \times \frac{\pi\hbar(1+\omega^2\tau_p^2 3/\pi^2)}{8\xi\tau_p T_0}. \qquad (17)$$

Figure 4 shows the spectral dependences of the ratio (Re $\sigma_\omega^{inter}$/Re$\sigma_\omega^{intra}$) for the GL–$MoS_2$ and GL-$WSe_2$ heterostructures calculated for different injection currents using equation (17). It is assumed that $T_0 = 26$ meV and $\mu_a = 100$ meV. This implies that the interband radiative transitions from the GL conduction band to the valence band with the emission of photons (surface plasmons) surpass the intraband processes of the Drude absorption. Thus, the GL-based heterostructures with the BLs under consideration support sufficiently strong electron and hole injection and can be used in the THz superluminescent and laser diodes. As shown by the calculations for the similar heterostructures with moderately doped GLs ($\mu_a = 50$ meV), the ratio $\mathrm{Re}\sigma_\omega^{inter}/\mathrm{Re}\sigma_\omega^{intra} > -1$, so that the dynamic conductivity is positive for all photon energies under consideration despite the population inversion (see figure 3). The main factor limiting the red shift of the spectral characteristics of the heterostructures under consideration is the interband (Drude) absorption that increases dramatically with decreasing $\hbar\omega$. Such a shift requires longer carrier scattering time $\tau_p$. This means that these device structures used for the THz sources might require the design optimization.

## 6. Comments

For the parameters corresponding to figure 4, $\mathrm{Re}\sigma_\omega^{inter}/\mathrm{Re}\sigma_\omega^{intra} < -1$, i.e., the net dynamic conductivity is negative in a wide spectral range (30–80 meV or 7–20 THz). Hence, the heterostructures considered above could be used for super–luminescent and laser diodes generating the 7–20 THz modes (both photonic and plasmonic [13, 14]) propagating in the GL in-plane direction (along the axis $y$) provided the proper reflection condition

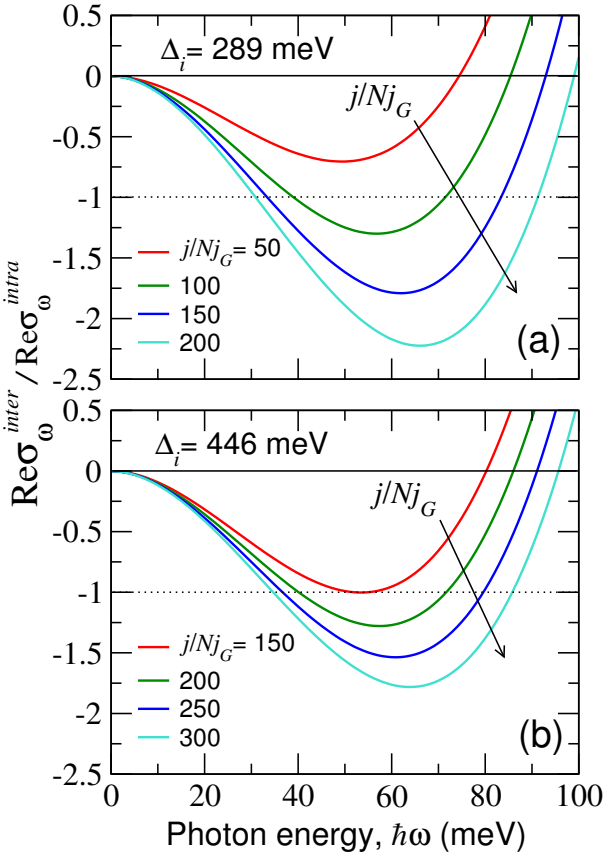


**Figure 4.** Spectral characteristics of the ratio of the real parts of the 2DEHP dynamic interband and intraband conductivities at different normalized injection currents for (a) GL-$MoS_2$ and (b) GL-$WSe_2$ heterostructures ($\mu_a = 100$ meV).

from the edges or the distributed feed-back structures (as, for example, in [10]).

At relatively low bias voltages $U < U_{bi}$, where $U_{bi}$ is the built-in voltage between the $p^+$- side contact and $n^+$-vertical contact, the electron injected current density is of the thermionic origin. Here $j_{max} = eN_d v_T$, $N_d$ is the donor density in the $n^+$-EL, and $v_T$ is thermal electron velocity. At $U > U_{bi}$, $j$ is limited by the electron and donor space charge in the n-EL or by the electron scattering in this layer (resistance limited injection). This case corresponds to the band diagram shown in figure 1(b). At a relatively large $U$, $j$ tends to saturate at $j_{sat} \simeq j_{max}$.

Assuming $N_d = 10^{18}\text{cm}^{-3}$ and $v_T = 10^7$ cm/s, we find $j_{sat} \simeq 1.6 \times 10^5$ A cm$^{-2}$. This quantity is much larger than $j_G \simeq 1.6 \times 10^2$ A cm$^{-2}$ (as estimated in Appendix A). This implies that the vertical emitter can provide a fairly strong injection pumping ($j/Nj_G \gg 1$) for a large number of the GLs. Assuming that $j \lesssim j_{sat}$ and $j/Nj_G \sim 100-300$ (as in figure 3), we find that a sufficiently strong injection pumping can be realized if $N \lesssim N_{max} = 3-10$.

In the case of the thermionic electron injection, the effective temperature of the electrons injected into the GLs $T_E$ can be somewhat lower than $T_0$ (the Peltier effect cooling). At the tunneling injection (see figure 1(c)), $T_E \simeq T_0$. In the case, of the space-charge or resistance limited injection, $T_E$ only slightly exceeds $T_0$ for a moderate number of the GLs N ($N \lesssim N_{max}$) (in agreement with the analysis given in [22]).

We neglected small potential variations across the BLs. Therefore, the BL bands shown in figures 1(b) and 1(c) are flat. In reality, some imbalance in the electron and hole densities in the GLs leads to the GL charging, especially for the GL adjacent to the n-EL. Nearly the entire voltage drop is between the n-EL and the top GL. As was shown previously [22], even a small surface charge (a small difference between $\Sigma_e$ and $(\Sigma_h - \Sigma_a)$) is sufficient to prevent the emitter electric field from a substantial penetration to the heterostructure bulk.

## 7. Conclusions

We presented a modeling and analysis for THz superluminescent and laser diodes based on multiple graphene layer-multiple van der Waals barrier layer structures with the diagonal carrier injection scheme of lateral hole injection from the side contacts and vertical

electron injection through the hetero-barriers. The developed model showed the effect of lateral hole injection on the overall carrier heating and promoting the carrier population inversion and the resultant negative dynamic conductivities. In conclusion, the multiple GL-BL heterostructures using the vdW materials (like MoS2 and WSe2) enable the THz injection superluminescent and laser diodes operating in the frequency range between 1 and 20 THz. A sufficiently strong GL doping (or the inter-GL BL doping) weakens the electron-hole plasma heating by the injected current enabling the interband population inversion and the negative dynamic conductivity. This allows using many barrier layer materials with relatively large band offsets for the THz sources under consideration. The combination of the vertical and lateral injection is superior for the optimized design and enables using up to 10 GL/BL layers connected in parallel for higher power.

**Acknowledgments**

The Japan Society for Promotion of Science (KAKENHI #16H02336), Japan; RIEC Nation-Wide Cooperative Research Project #H31/A01), Japan; The work at RPI was supported by the US Army Research Laboratory Cooperative Research Agreement (Project Monitor Dr. Meredith Reed) and by the US Office of Naval Research (Project Monitor Dr. Paul Maki), USA.

## Appendix A. Rate equations for the density and energy of the 2DEHP

For a relatively small number of the GL (see below), the capture rate of the injected holes into each GL and the pertinent power are equal to $(j/eN)$ and $(j/eN)\Delta_i$, respectively, where $\Delta_i = \Delta_V + 3T_E/2$ ($T_E \simeq T_0$ is the hole temperature in the emitter), the balance equations can be presented as

$$R^{inter} = \frac{j}{eN},\ \hbar\omega_0(R^{inter}+R^{intra}) = \frac{j}{eN}\Delta_i. \quad \text{(A1)}$$

Using the general formulas for the pertinent probabilities [49] and singling out the exponential factors, the rate of the recombination-generation processes and the rate of the energy relaxation in the 2DEHP in each GL associated with the emission and absorption of the optical phonons are given by

$$R^{inter} = \frac{\Sigma_0}{\tau_{opt}^{inter}}\left[\left(1+\frac{1}{\mathcal{N}_0}\right)\exp\left(\frac{\mu_e+\mu_h-\hbar\omega_0}{T}\right)-1\right], \quad \text{(A2)}$$

$$R^{intra} = \frac{\Sigma_0}{\tau_{opt}^{intra}}\left[\left(1+\frac{1}{\mathcal{N}_0}\right)\exp\left(-\frac{\hbar\omega_0}{T}\right)-1\right] \quad \text{(A3)}$$

Here $\mathcal{N}_0 = [\exp(\hbar\omega_0/T_0)-1]^{-1}$, $\hbar\omega_0$ and $T_0$ are the energy of optical phonons in the GLs and their effective temperature. The quantity $\Sigma_0/\tau_{opt}^{inter}$ is the generation rate of the electron-hole pairs in GL due to the absorption of the optical phonons in equilibrium (at room temperature, $\Sigma_0/\tau_0^{inter} \simeq 10^{21}$ cm$^{-2}$ s$^{-1}$ (hence, $j_G = e\Sigma_0/\tau_0^{inter} \simeq 1.6\times10^2$ A cm$^{-2}$), whereas $\tau_{opt}^{inter}$ is estimated as $\tau_{opt}^{inter} \simeq \tau_0\exp(\hbar\omega_0/T_0)$, where $\tau_0$ is the characteristic time of the optical phonon spontaneous emission. Equations (A2) and (A3) are valid if the optical phonon system remains close to equilibrium with the temperature of the lattice (thermostat) $T_0$. This takes place when the decay time of optical phonons in GLs into acoustic phonons is sufficiently small [49].

## Appendix B. Electron injection into the GLs

For the quasi-neutral electron-hole system including all the 2DEHPs, the density of

the electrons, $n$, propagating across the heterostructures can be described by the diffusion equation:

$$D\frac{d^2n}{dz^2} = \frac{n}{\tau_r} + \sum_{k=1}^{N} sn\delta[z-(k-1)d]. \qquad \text{(B1)}$$

Here $D$ and $\tau_r$ are the electron diffusion coefficient and recombination time in the barrier material, $s$ is the electron capture velocity into the GL, and $d$ is the thickness of the BLs. The second term in the right-hand side of equation (B1) describes the capture of the injected electrons crossing the GLs due to the interaction with the phonons and the holes in the GLs (see, for example, [46]). The plane of the GL (with the index $k = 1$) adjacent to the n-EL corresponds to the interface between the n-EL and this GL. The boundary conditions for equation (B1) are: $-D(dn/dz)|_{z=0} = j/e$, $-D(dn/dz|_{z=(N-1)d} = sn|_{z=(N-1)d}$, where $j$ is the density of the vertically injected hole current (in A cm$^{-2}$), $e = |e|$ is the electron charge, $N$ is the number of the GLs, so that $d_N = Nd$ is the net thickness of the heterostructure in the vertical direction (in the $z$ - direction as shown in figure 1). This value $j$ is related to the linear density, $J$, of the laterally injected electrons as $J = jL$ (in A cm$^{-1}$) with $L$ being the length of the GL, i.e., the spacing between the side contacts. The above boundary conditions correspond to the injection from the n-EL and the reflection from the substrate.

The effective diffusion length corresponding to equation (B1), can be estimated as $l_D = \sqrt{D(\tau_R^{-1} + s/d)^{-1}}$. If the electron recombination in the BLs is weak, at the condition $l_D \gtrsim d_N = Nd$ the nonuniformity of the injected hole spatial distribution can be disregarded. The latter inequality is satisfied for $N \gtrsim \sqrt{D/sd} = N_{max}$. If $N < N_{max}$, the rate of the electron capture, $j/eN$, into the GLs is approximately equal for all GLs. For $d = 10^{-6}$ cm, $s = 10^5$ cm/s, and $D = 10 - 100$ cm$^2$s$^{-1}$, the number of the GL in the device structures under consideration is limited by $N_{max} \simeq 10 - 30$. In the opposite case, i.e., in the heterostructures with too large number of the GLs, the GLs near the substrate are weakly pumped. This can suppress the population inversion in the GLs near the substrate.

## References


[1] Bonaccorso F, Sun Z, Hasan T and Ferrari A C 2010 Graphene photonics and optoelectronics *Nat. Photon.* **4** 611–622

[2] Ryzhii V, Ryabova N, Ryzhii M, Baryshnikov N V, Karasik V E, Mitin V and Otsuji T 2012 Terahertz and infrared photodetectors based on multiple graphene layer and nanoribbon structures *Opto-Electron. Rev.* **20** 15–25

[3] Bao Q and Loh K P 2012 Graphene photonics, plasmonics, and broadband optoelectronic devices *ACS Nano* **6** 3677–3694

[4] Tredicucci A and Vitiello M S 2014 Device concepts for graphene-based terahertz photonics *IEEE J. Sel. Top. Quantum Electron.* **20** 8500109

[5] Koppens F H L, Mueller T, Avouris Ph, Ferrari A C, Vitiello M S and Polini M 2014 Photodetectors based on graphene, other two-dimensional materials and hybrid systems *Nat. Nanotech.* **9** 780–793

[6] Ryzhii M and Ryzhii V 2007 Injection and population inversion in electrically induced p–n junction in graphene with split gates *Jpn. J. Appl. Phys.* **46** L151–L153

[7] Ryzhii V, Ryzhii M, Mitin V and Otsuji T 2011 Toward the creation of terahertz graphene injection laser *J. Appl. Phys.* **110** 094503

[8] Otsuji T, Tombet S B, Satou A, Ryzhii M and Ryzhii V 2013 Terahertz wave generation using graphene: toward new types of terahertz lasers *IEEE J. Sel. Top. Quantum Electron.* **19** 8400209

[9] Yadav D, Boubanga Tombet S, Watanabe T, Arnold S, Ryzhii V and Otsuji T 2016 Tera-

hertz wave generation and detection in double-graphene layered van der Waals heterostructures *2D Materials* **2** 045009

[10] Yadav D, Tamamushi G, Watanabe T, Mitsushio J, Tobah Y, Sugawara K, Dubinov A A, Satou A, Ryzhii M, Ryzhii V and Otsuji T 2018 Terahertz light-emitting graphene-channel transistor toward single-mode lasing *Nanophotonics* **7** 741–752

[11] Ryzhii V, Ryzhii M and Otsuji T 2007 Negative dynamic conductivity of graphene with optical pumping *J. Appl. Phys.* **101** 083114

[12] Ryzhii V, Ryzhii M, Satou A, Otsuji T, Dubinov A A and Aleshkin V Y 2009 Feasibility of terahertz lasing in optically pumped epitaxial multiple graphene layer structures *J. Appl. Phys.* **106** 084507

[13] Ryzhii V, Dubinov A A, Otsuji T, Mitin V and Shur M S 2010 Terahertz lasers based on optically pumped multiple graphene structures with slot-line and dielectric waveguides *J. Appl. Phys.* **107** 054505

[14] Dubinov A A, Aleshkin V Ya, Mitin V, Otsuji T and Ryzhii V 2011 Terahertz surface plasmons in optically pumped graphene structures *J. Phys.: Cond. Mat.* **23** 145302

[15] Boubanga-Tombet S, Chan S, Watanabe T, Satou A, Ryzhii V and Otsuji T 2012 Ultrafast carrier dynamics and terahertz emission in optically pumped graphene at room temperature *Phys. Rev. B* **85** 035443

[16] Li T, Luo L, Hupalo M, Zhang J, Tringides M C, Schmalian J and Wang J 2012 Femtosecond population inversion and stimulated emission of dense Dirac fermions in graphene *Phys. Rev. Lett.* **108** 167401

[17] Gierz I, Petersen J C, Mitrano M, Cacho C, Turcu I E, Springate E, Stöhr A, Köhler A, Starke U and Cavalleri A 2013 Snapshots of non-equilibrium Dirac carrier distributions in graphene *Nat. Mater.* **12**, 1119–1124

[18] Davoyan A R, Morozov M Yu, Popov V V, Satou A and Otsuji T 2013 Graphene surface emitting terahertz laser: diffusion pumping concept *Appl. Phys. Lett.* **103** 251102

[19] Ryzhii V, Semenikhin I, Ryzhii M, Svintsov D, Vyurkov V, Satou A and Otsuji T 2013 Double injection in graphene p-i-n structures *J. Appl. Phys.* **113** 244505

[20] Blicher A 1986 *Field-Effect and Bipolar Power Transistor Physics* (New York: Academic Press) p 104

[21] Wang L, Zhang Zi-H, and Wang N 2015 Current crowding phenomenon: Theoretical and direct correlation with the efficiency droop of light emitting diodes by a modified ABC model *IEEE J. Quant. Electron.* **51** 3200109

[22] Ryzhii V, Otsuji T, Ryzhii M, Karasik V E, and Shur M S 2019 Negative terahertz conductivity and amplification of surface plasmons in grapheneblack phosphorus injection laser heterostructures *Phys. Rev. B* **100** 115436

[23] Keyes R W 1953 The electrical properties of black phosphorous *Phys. Rev.* **92** 580–584

[24] Asahina H and A. Morita A 1984 Band structure and optical properties of black phosphorus *J. Phys. C: Solid State Phys.* **17** 1839

[25] Morita A 1986 Semiconducting black phosphorus *Appl. Phys. A* **39** 227–242

[26] Ling Xi, Wang H, Huang S, Xia F and Dresselhaus M S 2015 The renaissance of black phosphorus *PNAS* **112** 4523

[27] Liu H, Neal A T, Zhu Z, Luo Z, Xu X, Tománek D and Ye P D 2014 Phosphorene: An unexplored 2D semiconductor with a high hole mobility it ACS Nano **8** 4033–4041

[28] Qiao J, Kong X, Hu Z-H, Yang F and Li W 2014 High-mobility transport anisotropy and linear dichroism in few-layer black phosphorus *Nat. Comm.* **5** 4475

[29] Xia F, Wang H and Jia Y 2014 Rediscovering black phosphorous as an anisotropic layered material for optoelectronics and electronics it Nat. Comm. **5** 4458

[30] Guo Z, Zhang H, Lu S, Wang Z, Tang S, Shao J, Sun Z, Xie H, Wang H, Yu X-F, and Chu P K 2015 From black phosphorus to phosphorene: Basic solvent exfoliation, evolution of Raman scattering, and applications to ultrafast photonics *Adv. Funct. Mat.* **25** 6996

[31] Batmunkh M, Bat-Erdene M and Shapter J G 2016 Phosphorene and phosphorene-based materials - prospects for future applications *Adv Mater.* **28** 8586–8617

[32] Engel M, Steiner M and Ph. Avouris Ph 2014 A black phosphorus photo-detector for multispectral high-resolution imaging *Nano Lett.* **14** 6414–6417

[33] Deng Y, Luo Z, Conrad N J, Liu H, Gong Y, Najmaei S, Ajayan P M, Lou J, Xu X and Ye P D 2014 Black phosphorus-monolayer $MoS_2$ van der Waals heterojunction p-n diode *ACS Nano*

**8** 8292

[34] Castellanos-Gomez A 2015 Black phosphorus: narrow gap, wide applications it J. Phys. Chem. Lett. **6** 4280–91

[35] Xu Y, Dai J and Zeng X C 2015 Electron-transport properties of few-layer black phosphorous *J. Phys. Chem. Lett.* **6** 1996–2002

[36] Ahmed F, Kim Y D, Choi M S, Liu X, Qu D, Yang Z, Hu J, Herman I P, Hone J, Yoo W J 2017 High electric field carrier transport and power dissipation in multilayer black phosphorus field effect transistor with dielectric engineering *Adv. Funct. Mater.* **27** 1604025

[37] Leong E, Suess R J, Sushkov A B, Drew H D, Murphy T E and Mittendorff M 2017 Terahertz photoresponse of black phosphorus *Opt. Express* **25** 12666–12674

[38] Cai Y, Zhang G and Zhang Y-W 2014 Layer-dependent band alignment and work function of few-layer phosphorene *Sci. Reps.* **4** 6677

[39] Liu B, Köpf M, Abbas A N, Wang X, Guo Q, Jia Y, Xia F, Weihrich R, Bachhuber F, Pielnhofer F,Wang H, Dhall R, Cronin S B, Ge M, Fang X, Nilges T, and Zhou C 2015 Black arsenicphosphorus: layered anisotropic infrared semiconductors with highly tunable compositions and properties *Adv. Mater.* **27** 4423–4429

[40] Tian He, Tan Z, Wu C, Wang X, Mohammad M A, Xie D, Yang Yi, Wang J, Li L-J, Xu J and Ren T-L 2014 Novel field-effect schottky barrier transistors based on graphene-$MoS_2$ heterojunctions *Sci. Reps.* **4** 5951

[41] Kim K, Larentis S, Fallahazad B, Lee K, Xue J, Dillen D C, Corbet C M and Tutuc E 2015 Band alignment in $WSe_2$graphene heterostructures *ACS Nano* **9** 4527-4532

[42] Zhang W, Wang Q, Chen Yu, Wang Z and Wee A T S 2016 Van der Waals stacked 2D layered materials for optoelectronics *2D Materials* **3** 022001

[43] Massicotte M, Schmidt P, Vialla F, Watanabe K, Taniguchi T, Tielrooij K J and Koppens F H L 2016 Photo-thermionic effect in vertical graphene heterostructures *Nat. Comm.* **7** 12174

[44] Rosencher E, Vinter B, Luc F, Thibaudeau L and Nagle J 1994 Emission and capture of electrons in multiquantum-well structures *IEEE J. Quantum Electron.* **30** 2875

[45] Aleshkin V Ya, Dubinov A A, Ryzhii M, Ryzhii V and Otsuji T 2015 Electron capture in van der Waals graphene-based heterostructures with WS2 barrier layers *J. Phys. Soc. Japan* **84** 094703

[46] Ryzhii V, Ryzhii M, Mitin V, Satou A and Otsuji T 2011 Effect of heating and cooling of photogenerated electron-hole plasma in optically pumped graphene on population inversion, *Jpn. J. Appl. Phys.* **50** 094001

[47] Rana F, George P A, Strait J H, Dawlaty J, Shivaraman S, Chandrashekhar M and Spencer M G 2009 Carrier recombination and generation rates for intravalley and intervalley phonon scattering in graphene *Phys. Rev. B* **79** 115447

[48] Golla D, Brasington A, Leroy B J and Sandhu A 2017 Ultrafast relaxation of hot phonons in graphene-hBN heterostructures *APL Materials* **5** 056101

[49] Balandin A A 2011 Thermal properties of graphene and nanostructured carbon materials *Nat. Mat.* **10** 569-581

[50] Pop E,Varsney V and Roy A K 2012 Thermal properties of graphene: Fundamentals and applications *MRS Bull.* **37**, 1273–1281

[51] Falkovsky L A and Varlamov A A 2007 Space-time dispersion of graphene conductivity *European Phys. J. B* **56** 281–284

[52] Hwang E H, Adam S and Sarma S D 2007 Carrier transport in two-dimensional graphene layers *Phys. Rev. Lett.* **98** 186806

[53] Vasko F T and Ryzhii V 2007 Voltage and temperature dependencies of conductivity in gated graphene *Phys. Rev. B* **76** 233404

[54] Svintsov D, Vyurkov V, Yurchenko S, Otsuji T and Ryzhii V 2012 Hydrodynamic model for electron-hole plasma in graphene *J. Appl. Phys.* **111** 083715

[55] Vyurkov V and Ryzhii V 2008 Effect of Coulomb scattering on graphene conductivity it JETP Lett. **88** 322-325

[56] Svintsov D, Ryzhii V, Satou A, Otsuji T and Vyurkov V 2014 Carrier-carrier scattering and negative dynamic conductivity in pumped graphene *Opt. Express* **22** 19873–19886

[57] Ryzhii V, Ponomarev D S, Ryzhii M, Mitin V, Shur M S and Otsuji T 2019 Negative and positive terahertz and infrared photoconductivity in uncooled graphene *Opt. Mat. Express* **9** 585–597

[58] Ryzhii V, Ryzhii M, Mitin V, Shur M S and Otsuji T 2020 Far-infrared photodetectors based on graphene/black-AsP heterostructures

*Opt. Express* **28** 2480–2498